Combining Thickness Information with Surface Tensor-based Morphometry for the 3D Statistical Analysis of the Corpus Callosum

Liang Xu[a], Olivier Collignon[d], Gang Wang[a,e], Yue Kang[c], Franco Leporé[f], Jie Shi[a], Yi Lao[c], Anand Joshi[g], Natasha Leporé[b,c,*], Yalin Wang[a,*]

[a] *School of Computing, Informatics, and Decision Systems Engineering, Arizona State University, Tempe, AZ, USA*
[b] *Department of Radiology, Children's Hospital Los Angeles, CA, USA*
[c] *Departments of Radiology & Biomedical Engineering, University of Southern California, CA, USA*
[d] *Center for Mind/Brain Science, University of Trento, Trento, Italy*
[e] *School of Computer Science and Technology, Ludong University, China*
[f] *Department of Psychology, University of Montreal, Montreal, QC, Canada*
[g] *Signal and Image Processing Institute, Brain and Creativity Institute, University of Southern California, Los Angeles, CA, USA*
[*] *Equal senior authors.*

Abstract. We propose a novel framework to capture a complete set of 3D morphological differences in the corpus callosum (CC) between two groups of subjects. The CCs are segmented from whole brain T1-weighted magnetic resonance images and modeled as 3D tetrahedral meshes. The callosal surface is divided into superior and inferior patches on which we compute a volumetric harmonic field by solving the Laplace's equation with Dirichlet boundary conditions. We adopt a refined tetrahedral mesh to compute the Laplacian operator, so our computation can achieve sub-voxel accuracy. Thickness is estimated by tracing the streamlines in the harmonic field. We combine areal changes found using surface tensor-based morphometry and thickness information into a vector at each vertex to be used as a metric for the statistical analysis. Group differences are assessed on this combined measure through Hotelling's T^2 test. The method is applied to statistically compare three groups consisting of: congenitally blind (CB), late blind (LB; onset > 8 years old) and sighted (SC) subjects. Our results reveal significant differences in several regions of the CC between both blind groups and the sighted group, and to a lesser extent between the LB and CB groups. These results demonstrate the crucial role of visual deprivation during the developmental period in reshaping the structural architecture of the CC.

1 Introduction

The corpus callosum (CC) is one of the most highly studied subcortical structure in post-processing analyses of magnetic resonance images. This is in part due to its involvement in numerous disorders that affect the brain. The splenium of the

CC carries fibers that connect visuo-spatial areas of the brain, and the isthmus is also involved in visuo-spatial processing, as it contains fibers connecting the posterior parietal areas, which fuse multimodality sensory information [1]. The CC undergoes extensive myelinization during development until adolescence, and waves of peak growth rates can be observed in the CC's of children of different ages [2]. Hence, studying the respective impact of congenitally (CB) versus lately acquired blindness (LB) on the anatomy of the CC provides a unique model to probe how experience at different developmental periods shapes the structural organization of the brain.

On the processing side, in T1-weighted magnetic resonance images (MRI), its high contrast difference from surrounding structures make accurate callosal segmentations straightforward for both manual and automatic methods. Additionally, its functional differentiation along an elongated sagittal axis has allowed researchers to focus on 2D analysis of the mid-sagittal section, allowing for simpler and faster numerical tools. Even so, it is clear that a 3D structural analysis can help visualization and may pick up some important information about the 3D structure of the CC that is discarded by 2D process.

We propose a novel 3D pipeline for the 3D analysis of the CC. While most studies have focussed on 2D representations of this structure, Wang et al. [3] compared the 3D CC of premature neonates to that of term-born controls. In that work, a surface grid was generated on the CC, and callosal thickness was computed as the distance from a medial axis. Statistical significance was assessed at each vertex on a vector containing the thickness and the deformation tensors from a multivariate tensor-based morphometry analysis (mTBM). The deformation tensors represent changes in area on the surface. However, for concave callosal surfaces, the medial axis is not well-defined and does not always have a biologically meaningful interpretation. Here we propose a new thickness computation to be combined with the standard mTBM analysis as in [3]. Given 3D tetrahedral meshes of the CC, we use the mesh based Laplacian operator to compute a harmonic field. The thickness is computed from the streamlines of the harmonic field. The estimated callosal thickness is well-defined, and may reflect the intrinsic 3D geometrical structure better than thickness derived from a medial axis and facilitate consistent cross-subject comparisons.

In the field of computational anatomy, tensor-based morphometry (TBM) [4, 5] and more recently its multivariate extension, mTBM [6, 7], have been used extensively to detect regional differences in surface and volume brain morphology between groups of subjects. Here we focus more specifically on mTBM on the callosal surface. Prior work [6] combining mTBM with other statistics such as the radial distance has significantly improved statistical power. Intuitively, thickness and mTBM are complementary, as thickness describes distances roughly along the surface's normal direction, while mTBM detects surface dissimilarities, including differences in the surface metric tensor induced by the particular surface parameterization. So we argue that a combination of thickness and mTBM will offer a more complete set of surface statistics for callosal morphometry and hypothesize that they may boost statistical power to detect disease effects.

In this paper, we propose a combined multivariate morphometry statistics to study callosal differences associated with congenital-onset versus late-onset blindness. Our pipeline is applied on a data set consisting of: 14 congenitally blind (CB), 10 late blind (LB; onset > 8 years old) and 20 sighted control (SC) subjects. Prior 2D TBM analyses of the corpus callosum [7] revealed reductions in the ithmus and the splenium of the corpus callosum in early but not late blind compared to sighted controls. Comparisons of the early and late blind groups did not find any significant changes, though we hypothesize that they may be detected by our more powerful method. Additionally, [7] observed changes in the frontal lobes, though those were not reflected in the 2D analyses of the callosal regions connecting areas of the frontal lobes.

There are three main contributions in this paper. First, we propose an efficient method to compute the harmonic field with a tetrahedral mesh. Prior work on voxel-based brain thickness analysis [8, 9] relied on a three-dimensional cubic voxel grid to solve partial differential equations (PDE) in the potential field. However, due to the restrictions on the grid resolution which cannot precisely characterize the curved cortical surfaces in MR images, the measurement accuracy from this method is low and sensitive to noise. Our approach overcomes the defect of the limited grid resolution by adopting a high quality, adaptive tetrahedral mesh [10] and a finite element based Laplacian operator [11]. Compared with prior work [8, 9], our PDE solving computation can achieve sub-voxel accuracy. Second, we propose a multivariate statistics by combining the callosal thickness computed from our new method and mTBM. Lastly, through multiple comparison, we identify statistically significant areas on CC between the CB and LB groups. This discovery may help further our understanding of brain plasticity and in the long term, improve the effectiveness of rehabilitation techniques for blind individuals.

2 3D Callosal Thickness Computation with Harmonic Field

2.1 Solving Laplace's Equation with Volumetric Laplacian Operators

Laplace's equation $\Delta f = \nabla^2 f = 0$ in 3D Cartesian coordinates takes the form:

$$(\frac{\partial^2}{\partial x^2} + \frac{\partial^2}{\partial y^2} + \frac{\partial^2}{\partial z^2}) f(x, y, z) = 0.$$

f is called harmonic if it satisfies the Laplace's equation with Dirichlet boundary conditions. The computed function is called the *harmonic field*. Assume there are two boundaries, B_0 and B_1, the harmonic field is computed by solving for the harmonic function $f_M : M \to \mathbb{R}$, such that

$$\begin{cases} \Delta f_M(p) = 0 \; \forall p \notin B_0 \cup B_1 \\ f_M(p) = 0 \quad \forall p \in B_0 \\ f_M(p) = 1 \quad \forall p \in B_1 \end{cases} \tag{1}$$

Eqn. 1 has been used to estimate the thickness of cerebral cortex [8, 12–14] and CC thickness on the mid-sagittal section [9]. Here we propose a finite element approach to solve Eqn. 1 and achieve sub-voxel accuracy on the boundaries. Compared with prior voxel-based scheme [8, 9, 12–14], our new work may overcome the numerical inaccuracy due to the limited resolution of 3D grid.

Practically, we use tetrahedra to represent the volume data. Suppose K is a simplicial complex, and $g : |K| \to \mathbb{R}^3$ a function that embeds $|K|$ in $\mathbb{R}^3$, then (K, g) is called a mesh. For a 3-simplex, it is a tetrahedral mesh, Te, and for a 2-simplex, it is a triangular mesh, Tr. Clearly, the boundary of a tetrahedral mesh is a triangular mesh, $Tr = \partial Te$.

Since the conventional harmonic energy is equivalent to the discrete harmonic energy [11] on a mesh, one may use the discrete Laplacian operator to minimize the harmonic energy. Here we adopt the Laplacian operator defined with tetrahedral mesh [11], as well as the following definitions.

Definition 1. *Suppose that edge $\{u, v\}$ is shared by n tetrahedra; thus it lies against n dihedral angles, θ_i, $i = 1, \ldots, n$. Denote l_i as the length of each edge that edge $\{u, v\}$ lies against in the domain manifold M, one can define the parameters $k_{u,v} = \frac{1}{12} \sum_{i=1}^{n} l_i \cot(\theta_i)$.*

Definition 2. *The* piecewise Laplacian *is the linear operator $\Delta_{PL} : C^{PL} \to C^{PL}$ on the space of piecewise linear functions on K, defined by the formula $\Delta_{PL}(f) = \sum_{\{u,v\} \in K} k(u, v)(f(v) - f(u))$.*

Definition 3. *Given a tetrahedral mesh, the* graph weight matrix *is defined as $S_{u,v} = \begin{cases} k_{u,v} & \exists e_{u,v} \\ 0 & \neg \exists e_{u,v} \end{cases}$, where $k_{u,v}$ is defined in Definition 2 [11]. Clearly, S is a sparse matrix and can be decomposed as $S = \begin{pmatrix} W_{VV} & W_{V\partial V} \\ W_{\partial VV} & W_{\partial V\partial V} \end{pmatrix}$, where V and ∂V represent the set of internal vertices and boundary vertices, respectively.*

Definition 4. *Under Dirichlet boundary conditions, the Laplacian matrix is $L_p = D_{VV} + D_{V\partial V} - S_{VV}$, where the diagonal matrix $D_{V\partial V} = diag(S_{V\partial V}\mathbf{e}_i)$, $\mathbf{e}_i$ is the ith column vector in an identity matrix, i.e., $(D_{V\partial V})_{ii}$ = the sum of i-th row in $W_{V\partial V}$.*

Definition 5. *With the discrete Laplacian operator definition, we compute the harmonic field with Dirichlet boundary conditions,*

$$L_p x = c, \tag{2}$$

where x is a $|u| \times 1$ vector ($|u|$ is the number of internal vertices). Note x only contains unknown function values on internal vertices, i.e. W_{VV}, as shown in the definition of L_p; and constant vector c is computed by $c_u = f_l^T W_{\partial VV} = \Sigma_{[v,w] \in M} f_l k_{v,w}$, where f_l is the specified function value on boundary vertices.

2.2 Thickness Profile Generation with the Harmonic Fields

Eqn. 2 is the discretized version of Eqn. 1. After computing the harmonic field f by solving x for internal vertices in Eqn. 2, we can compute the streamlines

to connect the two surfaces [8, 9]. Computationally, we construct a streamline as a parametric curves $u(s)$ with arc length parameter s. The thickness is defined as the total arc length of the streamline that traverses the CC from superior to inferior (or, alternatively, from inferior to superior) patches. Formally, we solve the following ordinary differential equation to construct the streamlines:

$$\begin{cases} u'(s) = \pm \frac{\nabla f(u(s))}{|\nabla f(u(s))|} \\ u(0) = \mathbf{x} \end{cases} \tag{3}$$

where $\mathbf{x}$ is a point on the starting surface patch and the streamline stops when it intersects the other surface patch. u' takes different sign based on the starting surface patch. Solving for Eqn. 1 using B_0 as either the superior or inferior surface, and B_1 as the other surface, we can compute the thickness at each point on superior and inferior surfaces, respectively.

3 Multivariate Morphometric Feature Computation

Alg. 1 and Fig. 1 illustrate the algorithm pipeline of our multivariate morphometry computation. In the following, we explain each step in details.

Step 1. Tetrahedral mesh and triangular mesh generation. Our meshes are generated by an adaptively sized tetrahedral mesh modeling method [10]. The method produces meshes conforming to the voxelized regions in the image by minimizing an energy function consisting of a smoothing term, a fidelity term and an elasticity term. Fig. 1(a) shows the binary image of a segmented corpus collosum and (b) shows its tetrahedral mesh. The boundary of the tetrahedral mesh gives a surface triangular mesh for the callosal surface (Fig. 1(c)).

Step 2. Surface registration and surface decomposition. The goal is to register CC surfaces and decompose them into two boundaries for thickness analysis. Given the long and thin structure of a CC surface, existing area-preserving spherical mapping based subcortical algorithms [15] may produce much distortion. For an accurate surface registration and decomposition, we adopt a holomorphic 1-form based method [6]. First, given a callosal surface, we label two consistent landmark curves at the caudal and rostral endpoints. They are biologically valid and consistent landmarks across subjects as shown in Fig. 1(d) (yellow lines). We call this process topological optimization. Given the callosal horizonal tube-like shape, these landmarks curves can be automatically detected by checking the extreme points along the first principal direction of the geometric moments of the surface. Secondly, we conformally map the callosal surface onto a rectangular planar domain with a holomorphic 1-form based conformal parameterization algorithm as in [6]. Fig. 1(e) illustrates the conformal parameterization by texture mapping the checkboard back to the surface. Finally, given two callosal surfaces S_1 and S_2 and their parameterizations, $\tau_1 : S_1 \to \mathbb{R}^2$ and $\tau_2 : S_2 \to \mathbb{R}^2$, we find a harmonic map $\tau : \mathbb{R}^2 \to \mathbb{R}^2$ between the parameter domains, such that:

$$\tau \circ \tau_1(S_1) = \tau_2(S_2), \tau \circ \tau_1(\partial S_1) = \tau_2(\partial S_2), \Delta\tau = 0.$$

Algorithm 1 Multivariate Morphometry of 3D Corpus Callosum.

Input: Binary image of segmented corpus callosum
Output: Morphometry features for each boundary vertex, including thickness and deformation tensors.
1. Build tetrahedral mesh from the binary image; build triangular mesh by computing the boundary of the tetrahedral mesh;
2. Register surfaces via holomorphic 1-form method [6]; decompose a surface into superior and inferior patches by tracing iso-parametric curves;
3. Compute callosal thickness using the harmonic field;
4. Compute deformation tensors; construct the multivariate morphometry features by combining mTBM and thickness feature.

On the registered surfaces, we generate two iso-parametric curves which pass the extreme points on two lateral sides. By cutting along these two curves and removing their attached triangles (also the tetrahedra in the tetrahedral mesh), we produce superior and inferior surface patches, which are used for the callosal thickness computation. (Fig. 1(f) shows the segmented superior and inferior surface patches (superior patch in blue and inferior patch in yellow).

Step 3. Callosal thickness computation. Similar to prior CC morphometric approaches with 2D Laplace's equations [9, 16], our approach computes the 3D Laplace's equation with an efficient discrete Laplacian operator. The details of the algorithm is described in Sec. 2. Fig. 1(g) shows how to compute the streamlines from the harmonic fields. We generate level set surfaces of the harmonic fields and the stream lines are computed by tracing their normal directions. (h) shows the color maps of the computed thickness profile on the callosal surfaces.

Step 4. Multivariate morphometry feature computation. Our complete multivariate morphometry feature consists of deformation tensors in log-Euclidean space and callosal thickness. Given two triangles, $[v_1, v_2, v_3]$ and $[w_1, w_2, w_3]$, first, we isometrically embed them onto the plane $\mathbb{R}^2$; the planar coordinates of the vertices of v_i, w_j are denoted using the same symbols v_i, w_j. Then we explicitly compute the Jacobian matrix J,

$$J = [w_3 - w_1, w_2 - w_1][v_3 - v_1, v_2 - v_1]^{-1}.$$

The deformation tensor can be defined as $S = (J^T J)^{\frac{1}{2}}$. Instead of analyzing shape change based on the eigenvalues of the deformation tensor, a new family of metrics, the "Log-Euclidean metrics" [17] is used in multivariate tensor-based morphometry (mTBM). This conversion makes computations on tensors easier to perform and statistical parameters can then be computed easily using the standard formulae for Euclidean spaces.

To compute group differences with multivariate morphometry features, we then apply Hotelling's T^2 test on sets of multivariate morphometry values. Given two groups of $n \times 1$-dimensional vectors, $S_i, i = 1, 2, , p, T_j, j = 1, 2, , q$, we use the Mahalanobis distance M to measure the group mean difference,

$$M = \frac{N_S N_T}{N_S + N_T}(\bar{S} - \bar{T})\Sigma^{-1}(\bar{S} - \bar{T})$$

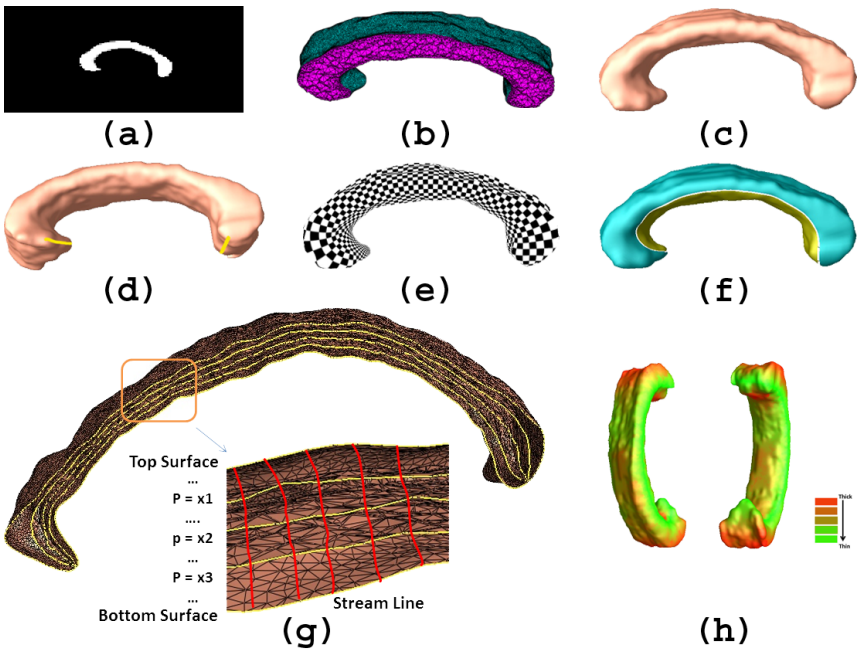

Fig. 1: Algorithm Pipeline illustrated by intermediate results.

where N_S and N_T are the number of subjects in the two groups, $\bar{S}$ and $\bar{T}$ are the means of the two groups and Σ is the combined covariance matrix of the two groups [18]. Since the statistic M is univariate, our analysis does not introduce any bias because of the increase in the number of variables.

4 Experimental Results

Our data set consists of 14 CB, 10 LB and 20 SC adult subjects scanned on a 3T MPRAGE Siemens Tim Trio MRI Scanner quality. Images were aligned and scaled to the ICBM-53 brain template (International Consortium for Brain Mapping) with the FLIRT software [19], using a 9-parameter linear transformations (3 translations, 3 rotations and 3 scales). Then we manually segmented the CCs with Insight Toolkit's SNAP program [20]. Tracings were performed in the registered template space by a trained investigator (Y.K.) and the results were checked by an experienced neuroscientist (F.L.). We consulted neuroanatomical references of the corpus callosum to help guide the placement of the contours. Fig. 2 shows some segmented results.

Then we apply Alg. 1 on the obtained binary images. Specifically, we generate tetrahedral meshes [10], compute conformal grids on their surface, register surfaces with constrained harmonic map and segment them into superior and inferior patches. We then estimate mTBM and the thickness (THK) at each vertex between the two patches using the harmonic field. Similar to the practice in [18], we also linearly covary the multivariate statistics at each pixel with subject age

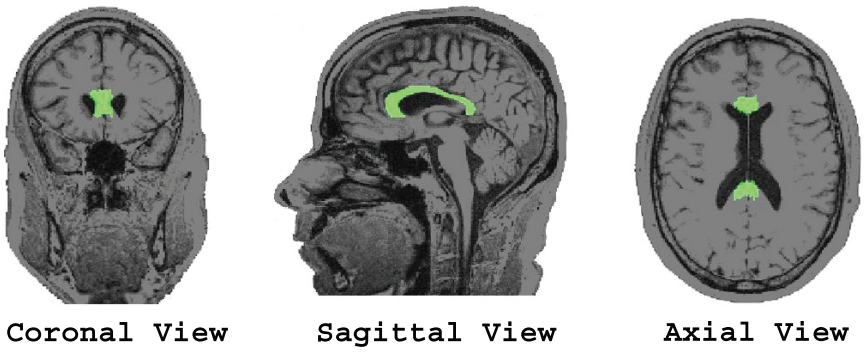

Fig. 2: Manually segmented callosal structure overlayed on an MRI image.

and gender information. The covaried statistics are used for a group difference study. For the group difference test, we run a permutation test with 5000 random assignments of subjects to groups to estimate the statistical significance (p-maps) in surface morphometry [6].

Fig. 3 shows uncorrected p-maps for three group difference studies. To explore whether our multivariate statistics provide extra power when combining thickness with mTBM, in each experiment, we also conducted three additional statistical tests using the thickness and different tensor-based statistics derived from the Jacobian matrix. The other statistics we studied are: (1) the thickness (THK) itself; (2) the determinant of Jacobian matrix; and (3) the mTBM. For statistics (1) and (2), we applied a Student's t-test to compute the group mean difference at each surface point. In case (3) and for our new combined measure, we used Hotelling's T^2 statistics to compute the group mean difference. In all sets of results, we detected significant areas around splenium areas for the combined measure. The CB also show significant changes in the body of the CC.

All group difference p-maps were corrected for multiple comparisons using the false discovery rate method (FDR) [21]. The FDR method determines the *critical p-value*, which is the highest threshold p-value that controls the FDR at the given threshold, e.g. 5%. To rank which clinical measures were most strongly associated with callosal morphology, we created cumulative distribution function (CDF) plots of the resulting uncorrected p-values. The critical p-value, which is the highest non-zero point at which the CDF plot intersects the $y = 20x$ line, represents the highest statistical threshold for which at most 5% false positive are expected in the map. If there is no such intersection point (other than the origin), there is no evidence to reject the null hypothesis. Also, steeper CDFs show stronger effect sizes. FDR results are shown in Fig. 4. All measures are significant for the CB vs. controls, while only our new combined measure falls above the $y = 20x$ line in the case of LB vs. controls.

Note that our results are consistent with previous work [7] and with the hypothesis that splenium regions should be affected in all blind groups, but more so in the CB. Our results are also consistent with another DTI tractography study [22], which found fractional anisotropy was significantly reduced in the

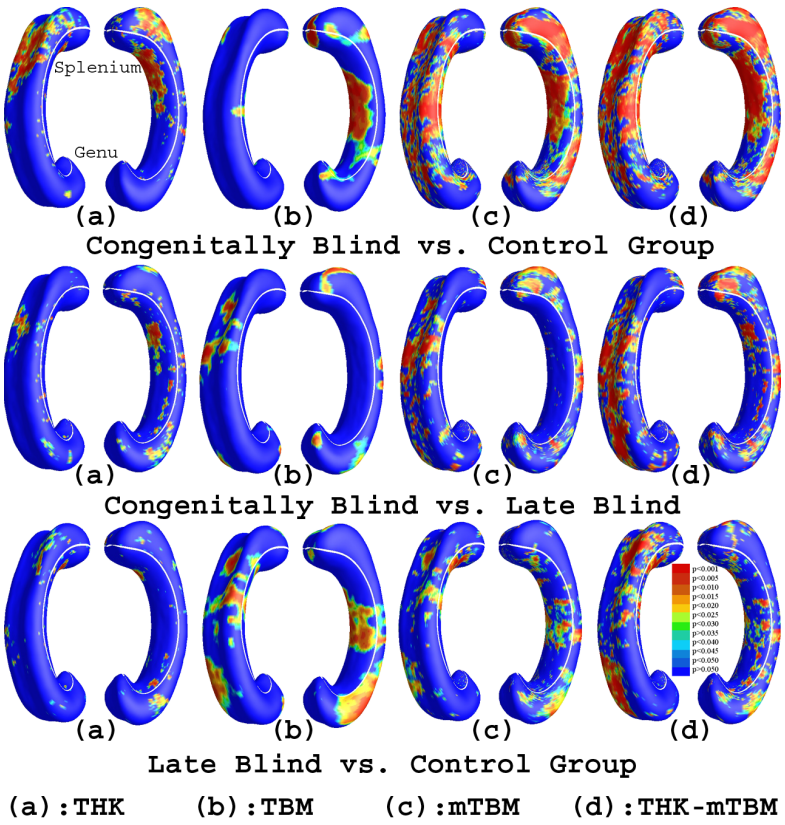

Fig. 3: Comparison of p-maps with four statistics on 3 different group difference studies. Non-blue colors show vertices with statistical differences, at the 0.05 level, uncorrected. The combined multivariate statistics outperformed all three individual statistics (the critical p-values for these maps are shown in Fig. 4).

splenium of CB subjects. The splenium is primarily composed of fibers connecting the visuo-spatial areas of the brain. The differences seen here may be due to reduced myelination of these fibers in the absence of visual input.

In addition, with our novel multivariate statistics, we found changes in the body of the CC in the LB group while no such difference was detected in [7]. In the late blind subjects, the process of myelination is relatively advanced, so that the structure of the corpus callosum may not be that strongly influenced by the loss of visual perception. Our new discovery, generally consistent with this understanding, may provide additional insights to the myelination and cortical plasticity process. More importantly, these results also suggest that the newly proposed multivariate morphometry has more detection power in terms of effect size, likely because it captures callosal thickness and more directional and rotational information when measuring geometric differences.

In future, we will combine and correlate our multivariate statistical framework with other MRI imaging systems, such as cortical morphometry and diffu-

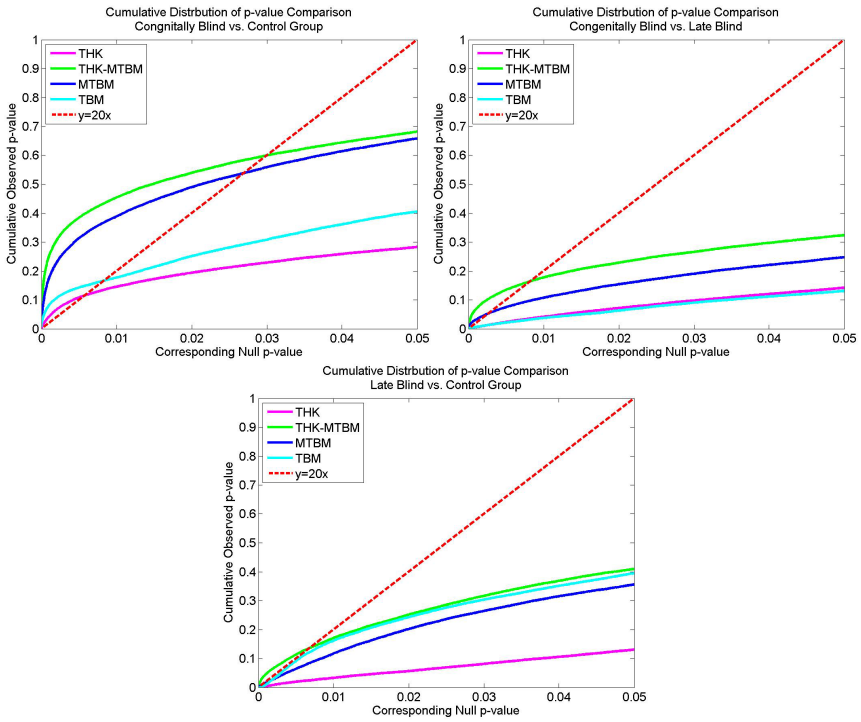

Fig. 4: The cumulative distributions of the p-values for difference detected between three diagnostic groups (CB, LB and SC) for all four statistics. The critical p-values are the intersection points of the curves and the $y = 20x$ line. The new multivariate statistics achieved the highest critical p-values in all 3 comparisons.

sion tensor imaging (DTI) tractography, to advance our understanding of blindness and improve the effectiveness of rehabilitation techniques and life quality for blind individuals.

References

1. Hofer, S., Frahm, J.: Topography of the human corpus callosum revisited–comprehensive fiber tractography using diffusion tensor magnetic resonance imaging. Neuroimage **32**(3) (Sep 2006) 989–994
2. Hua, X., Leow, A.D., Levitt, J.G., Caplan, R., Thompson, P.M., Toga, A.W.: Detecting brain growth patterns in normal children using tensor-based morphometry. Hum Brain Mapp **30**(1) (Jan 2009) 209–219
3. Wang, Y., Panigrahy, A., Shi, J., Ceschin, R., Nie, Z., Nelson, M.D., Leporé, N.: 3D vs. 2D surface shape analysis of the corpus callosum in premature neonates. In: MICCAI workshop on Paediatric and Perinatal Imaging, Nice, France (2012)
4. Davatzikos, C.: Spatial normalization of 3D brain images using deformable models. J Comput Assist Tomogr **20**(4) (1996) 656–665
5. Chung, M.K., Worsley, K.J., Paus, T., Cherif, C., Collins, D.L., Giedd, J.N., Rapoport, J.L., Evans, A.C.: A unified statistical approach to deformation-based morphometry. Neuroimage **14**(3) (Sep 2001) 595–606

6. Wang, Y., Song, Y., Rajagopalan, P., An, T., Liu, K., Chou, Y.Y., Gutman, B., Toga, A.W., Thompson, P.M.: Surface-based TBM boosts power to detect disease effects on the brain: An N=804 ADNI study. Neuroimage **56**(4) (2011) 1993–2010
7. Leporé, N., Voss, P., Lepore, F., Chou, Y.Y., Fortin, M., Gougoux, F., Lee, A.D., Brun, C., Lassonde, M., Madsen, S.K., Toga, A.W., Thompson, P.M.: Brain structure changes visualized in early- and late-onset blind subjects. Neuroimage **49**(1) (Jan 2010) 134–140
8. Jones, S.E., Buchbinder, B.R., Aharon, I.: Three-dimensional mapping of cortical thickness using Laplace's equation. Hum Brain Mapp **11**(1) (Sep 2000) 12–32
9. Adamson, C.L., Wood, A.G., Chen, J., Barton, S., Reutens, D.C., Pantelis, C., Velakoulis, D., Walterfang, M.: Thickness profile generation for the corpus callosum using Laplace's equation. Hum Brain Mapp **32**(12) (Dec 2011) 2131–2140
10. Lederman, C., Joshi, A., Dinov, I., Vese, L., Toga, A., Van Horn, J.D.: The generation of tetrahedral mesh models for neuroanatomical MRI. Neuroimage **55**(1) (Mar 2011) 153–164
11. Wang, Y., Gu, X., Chan, T.F., Thompson, P.M., Yau, S.T.: Volumetric harmonic brain mapping. In: Biomedical Imaging: From Nano to Macro, 2004. ISBI 2004. IEEE International Symposium on. (Apr. 2004) 1275–1278
12. Schmitt, O., Bohme, M.: A robust transcortical profile scanner for generating 2-D traverses in histological sections of richly curved cortical courses. Neuroimage **16**(4) (Aug 2002) 1103–1119
13. Yezzi, A.J., Prince, J.L.: An Eulerian PDE approach for computing tissue thickness. IEEE Trans Med Imaging **22**(10) (Oct 2003) 1332–1339
14. Hutton, C., De Vita, E., Ashburner, J., Deichmann, R., Turner, R.: Voxel-based cortical thickness measurements in MRI. Neuroimage **40**(4) (May 2008) 1701–1710
15. Styner, M., Lieberman, J.A., McClure, R.K., Weinberger, D.R., Jones, D.W., Gerig, G.: Morphometric analysis of lateral ventricles in schizophrenia and healthy controls regarding genetic and disease-specific factors. Proc. Natl. Acad. Sci. U. S. A. **102**(13) (2005) 4872–4877
16. Herron, T.J., Kang, X., Woods, D.L.: Automated measurement of the human corpus callosum using MRI. Front Neuroinform **6** (2012) 25
17. Arsigny, V., Fillard, P., Pennec, X., Ayache, N.: Log-Euclidean metrics for fast and simple calculus on diffusion tensors. Magn. Reson. Med. **56**(2) (2006) 411–421
18. Leporé, N., Brun, C., Chou, Y.Y., Chiang, M.C., Dutton, R.A., Hayashi, K.M., Luders, E., Lopez, O.L., Aizenstein, H.J., Toga, A.W., Becker, J.T., Thompson, P.M.: Generalized tensor-based morphometry of HIV/AIDS using multivariate statistics on deformation tensors. IEEE Trans. Med. Imag. **27**(1) (2008) 129–141
19. Jenkinson, M., Smith, S.: A global optimisation method for robust affine registration of brain images. Med Image Anal **5**(2) (Jun 2001) 143–156
20. Yushkevich, P.A., Piven, J., Hazlett, H.C., Smith, R.G., Ho, S., Gee, J.C., Gerig, G.: User-guided 3D active contour segmentation of anatomical structures: significantly improved efficiency and reliability. Neuroimage **31**(3) (Jul 2006) 1116–1128
21. Benjamini, Y., Hochberg, Y.: Controlling the False Discovery Rate: A Practical and Powerful Approach to Multiple Testing. Journal of the Royal Statistical Society. Series B (Methodological) **57**(1) (1995) 289–300
22. Yu, C., Shu, N., Li, J., Qin, W., Jiang, T., Li, K.: Plasticity of the corticospinal tract in early blindness revealed by quantitative analysis of fractional anisotropy based on diffusion tensor tractography. Neuroimage **36**(2) (Jun 2007) 411–417